ERROR STUDIES FOR THE JAEA-ADS LINAC *

B. Yee-Rendon†, J. Tamura, Y. Kondo, F. Maekawa, S. Meigo and H. Oguri
Japan Atomic Energy Agency (JAEA), Tokai, Japan

Abstract

The JAEA-ADS linac is a CW proton accelerator with a beam current of 20 mA and final energy of 1.5 GeV. Most of the beam acceleration is achieved by using superconducting cavities to attain high acceleration efficiency at CW mode. The main (superconducting) linac is composed of five families of cavities (Half Wave Resonators, Single Spokes Resonators, and Elliptical cavities) with their respectively magnets (Solenoids and Quadrupoles). Due to the large beam power in the linac of 30 MW and the high reliability required for the ADS project, a robust beam optic designed is necessary to have a stable beam operation and control the beam loss power. The JAEA-ADS linac is composed of several sections and components; therefore, misalignments of these elements together with field errors enhance the beam loss rate and compromise the safety of the linac. To this end, an error linac campaign was launched to estimate the error tolerance of the components and implement a correction scheme to reduce the beam loss power around the linac. This paper discusses the error analysis for the JAEA-ADS linac and points out which are its most sensitive parts.

INTRODUCTION

To overcome the problems of the long-term and high level of radio-toxicity of nuclear waste, the Japan Atomic Energy Agency (JAEA) is designing an Accelerator Driven Subcritical System (ADS). The JAEA-ADS project consists of a 30 MW CW superconducting proton linac, a Spallation target, and an 800 MW thermal power subcritical reactor [1].

The JAEA-ADS linac is composed of a normal conducting section and a superconducting (SC) one. The former region produced the proton and accelerates the particles up to 2.5 GeV, and the latter provides the rest of the energy; thus, it is the longest and most complex part of the linac. Figure 1 presents the layout of the JAEA-ADS linac and provides details about the Radio-Frequency (RF) operation, energy transition, among others.

The JAEA-ADS linac is a high-intensity accelerator; therefore, it requires strict control of the beam loss to avoid the radio-activation of the structures, which results in radiation damages of the accelerator's components and a restriction for staff maintenance inside the tunnel. The first design was the so-called ideal machine, with no error, and its optimization was based to operate with a beam loss lower than the hand-on maintenance limit, 1 W/M, and a reduction of the beam halo and emittance growth [2–4]. To this end, multiparticle simulations were performed from the MEBT to end of linac by using TRACEWIN program [5]. Table 1 shows a summary of the relevant parameters for the MEBT and the main linac of the ideal machine case.

Table 1: Relevant Parameters of the MEBT and Main Linac for an Ideal Machine, with No Errors.

Parameters	
Particle	Proton
Final energy (GeV)	1.5
Beam current (mA)	20
Initial $\epsilon_{norm,rms,x}$ (π *mm mrad*)	0.20
Initial $\epsilon_{norm,rms,y}$ (π *mm mrad*)	0.21
Initial $\epsilon_{norm,rms,z}$ (π *MeV deg*)	0.07
Final $\epsilon_{norm,rms,x}$ growth (%)	14.8
Final $\epsilon_{norm,rms,y}$ growth (%)	16.1
Final $\epsilon_{norm,rms,z}$ growth (%)	7.0
Beam loss rate (1/m)	0
Total length (m)	464
Number of cavities	334
Number of magnets	174

ERROR STUDIES

As a next step towards the robustness of the lattice design, error studies were implemented. Element errors in magnets and cavities elements that integrated the lattice from the MEBT to the end of the linac were simulated using TRACEWIN program. Table 2 presents the lattice configuration of the MEBT and the different SC sections. S stands for the superconducting solenoid, F, Normal conducting Focusing quadrupole in the X plane, D, Normal conducting Defocusing quadrupole in the X plane, C, Cavity and B, Buncher Cavity.

Table 2: The Lattice Period Configuration at the JAEA-ADS Linac

Section	**Configuration**	Numbers of periods
MEBT	F-B-D-F-D-B	1
HWR	S-C	20
SSR1	S-C-C	53
SSR2	S-C-C-C	26
EllipR1	F-D-C-C-C	53
EllipR2	F-D-C-C-C-C-C	26

The element errors consisted in:

- Misalignments: transverse offset and rotations errors.
- Gradient errors in magnets.
- RF amplitude and phase fluctuations in cavities.

In addition, the errors were classified according to its duration time: Statics and Dynamic. The former errors

* Work supported by Subvention for ADS development.
† byee@post.j-parc.jp

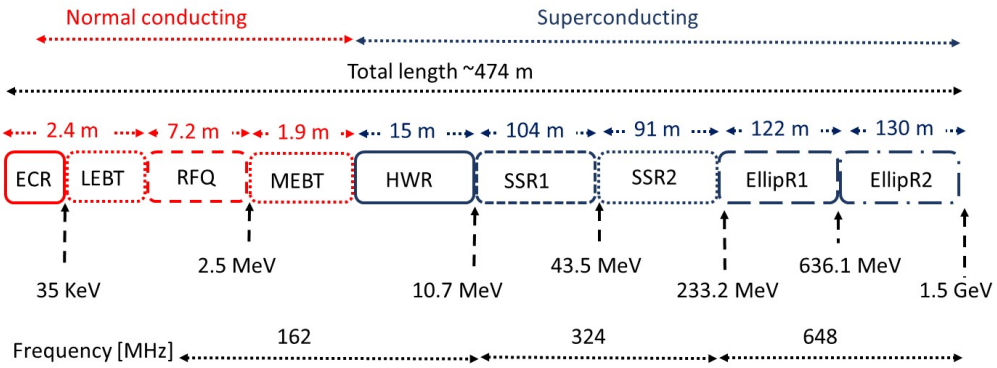

Figure 1: Layout of the JAEA-ADS.

were constant for a long period of time; thus, they were measured and compensated. Usually, they occurred during the installation or machine upgrade. The dynamics were random and abrupt; therefore, they remained uncompensated. These errors were caused by ground vibration, RF noise, etc., and were smaller than the static errors.

The error tolerance of the element must keep the beam losses below the limit hand-on maintenance. To this end, first, singles errors were applied. For each case, the amplitude error was increased in five steps and in each step the error's value was chosen uniformly plus-minus the maximum available error amplitude. Hundreds of runs with a beam distribution of 10^5 macroparticles were simulated for each step. The effects of the errors with respect to the ideal machine were quantified by:

- Beam loss
- Final normalized rms-emittance growth:

$$\Delta\epsilon/\epsilon_i = (\epsilon_{error} - \epsilon_{ideal})/\epsilon_{ideal}. \quad (1)$$

- Rms residual orbit:

$$R_{rms} = \sqrt{\frac{1}{N}\sum_{i=1}^{N} R_i^2 - \overline{R}}, \quad (2)$$

where

$$\overline{R} = \frac{1}{N}\sum_{i=1}^{N} R_i, \quad (3)$$

R is the beam gravity position in one of the three planes, N is the number of runs.

- Maximum beam envelope

Then, all the errors were combined. Finally, the error tolerances were set up by analyzing the results of the above quantities. The studies started with static errors and then with the dynamics.

RESULTS

The summary of the tolerances errors is reported in Table 3. The error's amplitudes were chosen after several interactions with multiparticle simulations to keep the beam loss condition. In particular, the error tolerances for the static cases were increased because of the implementation of the correction scheme. The tolerance values are similar to other high-intensity linacs [6–9].

The studies for the error type two, rotation errors in the horizontal plane for the magnets, is explained next to illustrate the procedure to compute the error tolerances. For the transverse misalignments only one plane was simulated for the single errors due to the transverse symmetry. However, for the combined errors, all the errors were applied in all the planes.

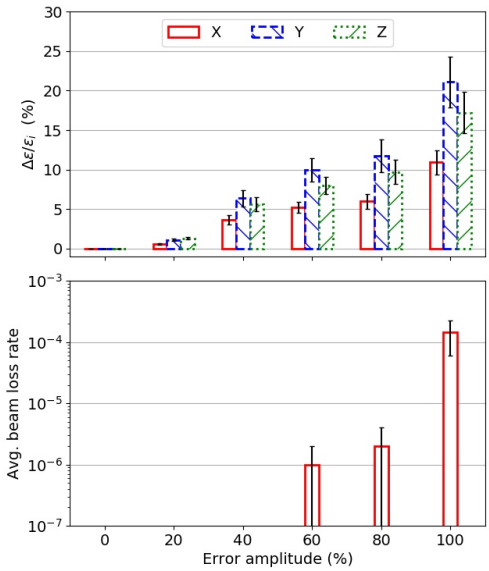

Figure 2: Error amplitude scan. The maximum emittance growth was below 25% (top). Beam loss appears from 60% of the error amplitude (bottom). Error bars represent the standard error of the mean.

Figure 2 presents the increase of normalized rms-emittance (top) and the average beam loss rate (bottom) as a function of the percentage of error amplitude. The plot shows that beam loss occurred for error values higher than 60% of the maximum error amplitude.

In addition, Fig. 3 shows the vertical rms residual displacement (top) at different error amplitudes and the average beam power lost (bottom) along the linac. Figs. 2 and 3 indicate that all the losses were located between HWR and

Table 3: Summary of the Static (S) and Dynamic (D) Element Errors for the JAEA-ADS

Error	Description	MEBT		HWR		SSR		EllipR	
		S	D	S	D	S	D	S	D
1	Magnet $\Delta X/Y$ (mm)	0.2	0.002	0.4	0.004	0.4	0.004	0.2	0.002
2	Magnet $\Delta\phi_{X/Y}$ (mrad)	0	0	2	0.02	1	0.01	0	0.
3	Magnet $\Delta\phi_Z$ (mrad)	2	0.02	0	0	0	0	2	0.02
4	Magnet Gradient (%)	0.5	0.1	0.5	0.1	0.5	0.1	0.5	0.1
5	Cavity $\Delta X/Y$ (mm)	0.4	0.004	0.5	0.005	0.5	0.005	0.5	0.005
6	Cavity $\Delta\phi_{X/Y}$ (mrad)	2	0.02	4	0.04	2	0.02	2	0.02
7	Cavity RF phase (deg)	1	0.5	1	0.5	1	0.5	1	0.5
8	Cavity RF Amplitude (%)	1	0.5	1	0.5	1	0.5	1	0.5

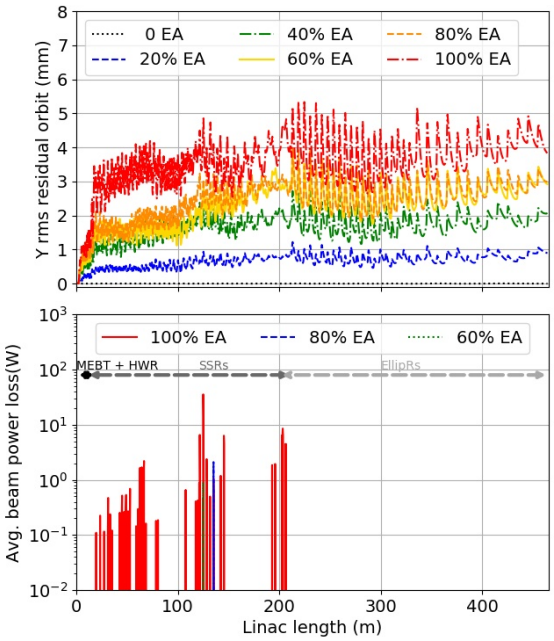

Figure 3: Vertical rms residual (top) and average beam power loss (bottom) along the linac for the different Error Amplitude (EA) cases. When the vertical rms over passed 3 mm, beam losses occurred, mainly, at the SSR's sections.

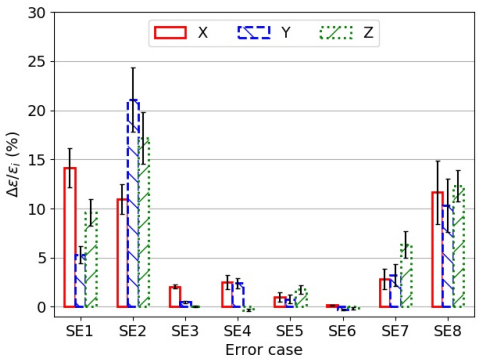

Figure 4: Emittance growth of the different single Static Errors (SE). Errors bars are the standard error of the mean.

SSR2 section. Beam losses occurred when the vertical rms residual orbit passed the 3 mm offset. The beam power lost for an error amplitude of 60% almost reached the limit of 1 W/m, the 80% case is slightly higher that the limit and the 100% is far beyond than the beam loss condition.

Figure 4 showed the summary of emittance growth for all the single static errors. The errors types one, two, seven and eight produced the highest emittance growth. However, only the errors one and two registered beam losses; in addition, these errors presented the highest rms residual orbit on the transverse plane. On the contrary, errors seven and eight produced the largest rms phase orbit offset.

From 80% of the misalignments error amplitude in magnets, the amount of beam power loss was beyond the safety limit. The results indicated that for the combined case, the beam losses will increase more. Thus, to keep beam loss condition two options were discussed: decreased the errors tolerances for the misalignments, or implemented a correction scheme.

A one-to-one correction scheme was implemented at the main linac to increase the error tolerance. In each period of the superconducting section, a pair of horizontal and vertical steering magnets associated with a pair of Beam Position Monitors (BPMs) downstream. The steerings applied a kick to compensate for the transverse offset of beam centroids in the BPMs [10]. For the orbit correction studies, the BPMs were simulated with an error of 100 μm to consider the common misalignment presented in the accelerators.

The efficacy of the correction scheme was evaluated by large simulations sets of 10^8 macroparticles. In each set, all element errors were applied simultaneously. The first case was the Static Element error With Out Correction Scheme (SEWOCS), and the second one was the Static Element error With Correction Scheme (SEWCS). The results are present in Table 4, Figs. 6 and 7.

For the dynamic cases, the same procedure for statics was applied. The error amplitude for the dynamic misalignments were 1% of the static errors. On the contrary, the gradient error was 20%, and the RF amplitude and phase were 50%, see Table 3.

Dynamic cases did not record any beam loss and the emittance growths, for each of the individual errors, were below 3% with respect to the ideal machine, see Fig. 5. Moreover,

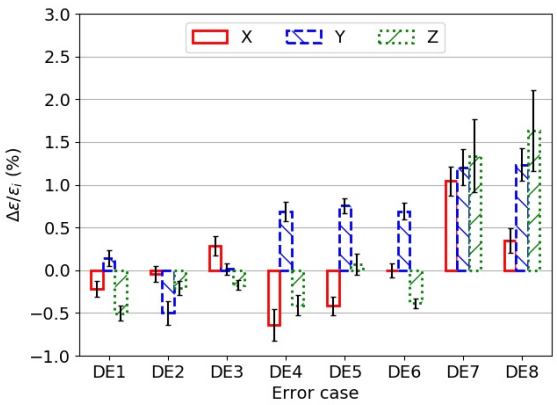

Figure 5: Emittance growth of the different single dynamic errors. Errors bars are the standard error of the mean.

for the first six cases the emittance increased was contained about $\pm 1\%$. In addition, the small error amplitudes changed the emittance growth equilibrium resulting in low negative values in some of the planes. On the contrary, the seven and eight cases, which have an error amplitude of 50% of the static case, registered increased in all the planes and showed the highest emittance growth. Finally, a large simulation of the combined errors of the Dynamic Element errors (DE), was simulated. Similar to the static cases, the results are shown in Table 4, Figs. 6 and 7.

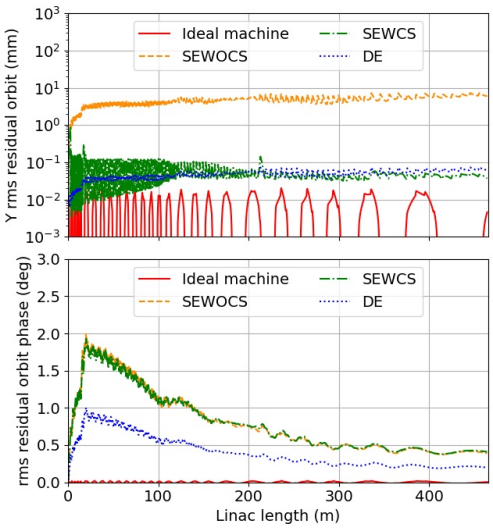

Figure 6: Rms residual orbit for the four cases, include the ideal machine. The top plot is the Y rms residual orbit, and the bottom is the rms residual phase.

Figure 6 shows the evolution of the rms residual orbit for the three cases. In addition, the values of the ideal machine were included for comparison. The top plot in Fig.6 presents the vertical rms beam orbit, horizontal plane presented the same behavior. The rms residual orbit was reduced below 0.3 mm, at the main linac, for the correction scheme. Because the MEBT does not have a correction scheme, that region has the largest transverse rms residual orbit for the SWECS's case. The DE studies did not produce large transverse rms residual orbit.

The bottom plot in Fig.6 shows the rms phase orbit displacements. The values of SEWOCS and SWECS are similar because the correction scheme only compensated for the transverse offset. The values of DE are smaller than the static ones; the reason is that RF amplitude and phase error were half with respect to the static cases.

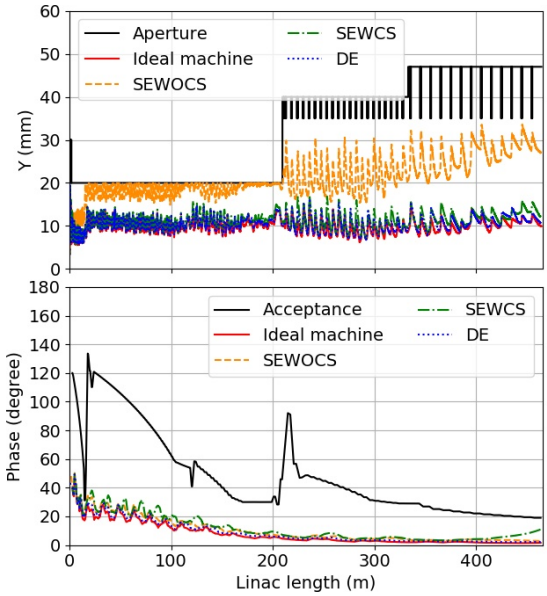

Figure 7: Maximum beam envelopes, for a cumulative statistic of 10^8 macroparticles, for the Y plane (top) and Phase (bottom). The SEWOCS shows that reached the SRRs's aperture (top). The acceptance has a bottle neck at the transition of HWR and SSR1 located about 27 m in length.

The maximum envelopes, equivalent to a beam distribution of 10^8 macroparticles, presented in Fig. 7 (top) shows clearly that for the SEWOCS the envelopes reached the aperture at the SSR's region. On the contrary, the other cases presented similar behavior as the ideal machine. Figure 7 (bottom) shows a significant phase acceptance of the linac; however, there is a bottle neck between HWR and SSR1 that could produce some particle fall outside the bucket.

Table 4 presents a summary of the average beam loss rate, emittance growth, rms residual orbit and maximum envelope for all the error cases and ideal machine. The results of the SEWOCS and SWECS evidenced the necessity of a correction scheme to increase the error tolerances, to keep with the safety limits for the beam operation. The SWECS presented an increase of the emittance growth less than 20% and the maximum envelopes were about 3% with respect to the ideal case. Finally, the dynamics errors had a small impact on the linac's performance. For example, the emittance growth, with respect to the ideal machine, was below 4%, and the increase of maximum envelopes was almost 1%.

Table 4: Summary of beam parameters for the different cases. The emittance growth is with respect to the initial emittance at MEBT (ϵ_0).

Parameter	**Ideal machine**	**SEWOCS**	**SEWCS**	**DE**
Avg beam loss rate (1/m)	0	0.032	0	0
$(\Delta\epsilon/\epsilon_0)_x$(%)	14.8	70.8	32.9	17.2
$(\Delta\epsilon/\epsilon_0)_y$(%)	16.1	67.8	31.6	18.9
$(\Delta\epsilon/\epsilon_0)_z$(%)	7.0	70.4	26.8	11.1
Max. rms residual X (mm)	0.03	7.63	1.35	0.07
Max. rms residual Y (mm)	0.01	7.30	0.91	0.07
Max. rms residual Phase (deg)	0.8	1.9	1.9	1.0
Max. Envelope X (mm)	23.5	36.0	24.2	23.5
Max. Envelope Y (mm)	19.2	33.6	19.6	19.4
Max. Envelope Phase (deg)	48.2	50.2	49.5	49.2

CONCLUSIONS

As a next step towards the development of JAEA-ADS lattice design, static and dynamic errors were simulated to compute the error tolerance of the lattice. Additionally, a one-to-one correction scheme was implemented to increase the error tolerances for static cases.

The impacts of the errors in the linac's performance were quantified by comparing the beam loss, emittance growth, rms residual orbit, and the maximum beam envelopes concerning ideal case. To this end, large simulation campaigns, a cumulative statistic of 10^8 macroparticles, were implemented to make the proper estimation of the previous variables.

The solenoid misalignments produced the highest transverse rms beam orbit displacements, above 3 mm. As a result, the SSR's sections recorded the largest amount of beam loss because of their small aperture of 40 mm. However, the transverse rms residual orbits were reduced, below 0.3 mm at the main linac, by the correction scheme. Moreover, an increase of the aperture size of the SSRs will be implemented for the next linac version.

The RF phase and amplitude errors were the main sources of the rms phase orbit offset. These displacements remained uncompensated by the present correction scheme. Nevertheless, the ratio of phase acceptance and the maximum beam phase is at least three times, but there is bottle neck between HWR to SSR1 that should be improved by adjusting the synchronous phase.

In summary, this study calculated tolerance error elements for the JAEA-ADS linac to operate with beam losses lower than 1 W/m in realistic, with elements errors, conditions.

ACKNOWLEDGMENTS

The authors would like to thank to the members of the JAEA-ADS and J-PARC linac groups for their comments and suggestions.

REFERENCES

[1] K. Tsujimoto *et al.*, "Neutronics design for lead-bismuth cooled accelerator-driven system for transmutation of minor actinide", *JNST*, vol. 41, no. 21, p. 21, Jan. 2004. doi:10.1080/18811248.2004.9715454

[2] B. Yee-Rendon *et al.*, "Beam Optics Design of the Superconducting Region of the JAEA ADS", *J. Phys. : Conf. Ser.*, vol. 1350, p. 012120, Nov. 2019. doi:10.1088/1742-6596/1350/1/012120

[3] B. Yee-Rendon *et al.*, "Cavity and Optics Design of the Accelerator for the JAEA-ADS Project", in *Proc. 16th Annual Meeting of Particle Accelerator Society of Japan. (PASJ2019)*, Kyoto, Japan, July-Aug. 2019. pp. 107-111.

[4] B. Yee-Rendon *et al.*, "Present Status of the R&D of the Superconducting Linac for the JAEA-ADS", *J. Phys. Soc. Jpn*, to be published.

[5] TraceWin, https://irfu.cea.fr/en/Phocea/Page/index.php?id=780

[6] G. Bellodi *et al.*, "Alignment and Field Error Tolerance in Linac4", CERN, Geneva, Switzerland, Rep. CERN-ATS-Note-2011-021, April. 2011.

[7] M. Esharqi *et al.*, "Statistical Error Studies in the ESS Linac", in *Proc. 5th Int. Particle Accelerator Conf. (IPAC'14)*, Dresden, Germany, June. 2014. pp. 3323-3325.

[8] Z. Li *et al.*, "Physics design of an accelerator for an accelerator-driven subcritical system", *Phys. Rev. ST Accel. Beams*, vol. 16, p. 080101, Dec. 2013. doi:10.1103/PhysRevSTAB.16.080101

[9] J. P. Carneiro and E. Podzeyev, "Beam Dynamics Studies of Misalignments and RF Errors for PIP-II", Fermilab, Illinios, U. S. A, Rep. PIP-II-doc-4083-v1, Feb. 2020.

[10] B. Mustapha *et al.*, "A Realistic Corrective Steering Algorithm: Formalism and Applications", in *Proc. 23rd Int. Particle Accelerator Conf. (PAC'09)*, Vancouver, Canada, May. 2009. pp. 3702-3704.